Accounts

Energy Transfer from Photoexcited Electronic States to the Thermal Modes

Masahide Terazima

Department of Chemistry, Graduate School of Science, Kyoto University, Kyoto, 606-8502

(Received September 1, 2000)

Energy transfer processes from a photoexcited ion and molecules to solvents were studied from the rate of the temperature rise of the solvent using several newly developed techniques: temperature grating, temperature lens, acoustic peak delay, and molecular heater–molecular thermometer methods. These energy transfer processes are closely related to the well-studied vibrational relaxation (cooling) process but the overall energy transfer process can be monitored by detecting the time course of the matrix heating. In aqueous solution, most of the energy of a photoexcited ion transfers to the thermal mode within 2–3 ps after the populational relaxation to a lower electronic state. In organic solvents, the process is described by roughly two kinetics: fast (≤ 1 ps) and slow (20–30 ps). This two-phase kinetics was explained by a simple thermalization model; the initial fast process represents the energy transfer to the doorway molecules in the first solvent shell molecules and the slower one represents the thermal diffusion process from the hot solvent molecules to the bulk solvent molecules. A new molecular heater-molecular thermometer integrated system is also described.

The energy flow process from solute to solvent is of major importance not only in chemistry but also in other fields of science such as laser ablation in industrial technology or biology, and has been a subject of extensive researches during the last two decades.[1,2] The excess energy due to the nonradiative transition between electronic states (internal conversion and/or intersystem crossing) will be first transferred to several energy-accepting vibrational modes, so that the total energy is conserved before and after the transition. The energy ultimately goes to the translational freedom (heating). This phenomenon is known as the photothermal effect and is one of the most commonly observed phenomena after the photoexcitation in condensed phase. Revealing the elementary step of this energy relaxation process has been one of the central topics in physical chemistry. The energy transfer process from the photoexcited molecule to the matrix has been studied so far by monitoring the population decay from highly excited vibrational states by the time-resolved Raman scattering, [3–7] transient IR spectroscopy,[8,9] the hot band detection of the solvent or solute molecules,[10–12] or the stimulated emission detection.[13,14] For example, intra- and inter-molecular energy transfer of 3-(1*H*-benzimidazol-2-yl)-7-(diethylamino)coumarin (coumarin 7) in C_2Cl_4 were studied by the fluorescence detection.[10a] The intermolecular energy transfer is found to take 7 ps. Molecular vibrational population relaxation rates for several vibrational modes of perylene in various solvents were reported using the stimulated emission technique.[13,14] They showed that the vibrational relaxation rate of perylene is slow, ranging from several hundreds to tens of picoseconds. The thermalization processes were also extensively studied using the molecular thermometer in solid polymers.[12] The vibrational cooling rate of azobenzene after photoisomerization was investigated by the time-resolved IR spectroscopy with a femtosecond time resolution.[8] The intermolecular energy transfer rate was found to be about 20 ps. A number of these results so far show that most of the vibrational relaxations of polyatomic molecules in solution are in a range of 100–10 ps. The temperature of the matrix rises because of the released energy from the highly excited vibrational states. Hence, it is reasonable to consider that the translational temperature rise also in a range of 100–10 ps even if the equilibrium process in the translational freedom is extremely fast. However, by using the direct temperature detection, I will show in this Account that this is not correct.

Compared with these rather extensive investigations of the vibrational cooling processes, studies of the heating process of the matrix, i.e., increase of the thermal energy, which is the ultimate energy-accepting mode in the condensed phase, are very rare. Detection of the temperature increase of the solvent is complementary to the cooling process and is very important for studying the overall energy transfer process from the electronic energy to the translational energy. So far, several photothermal detection methods have been developed for measuring the temperature increase.[15–25] However, although improvement on the sensitivity has been pursued extensively for a long time, it is not so much with respect to the time resolution. The photoacoustic method cannot detect the heat releasing process-

es faster than nanosecond order.[15–17] The time resolution of the thermal lens method has been widely recognized to be longer than 100 ns.[18–21] The transient grating (or thermal grating) method can provide a few tens of picoseconds time resolution,[22–25] but still the time resolution is not fast enough for revealing the initial step of the thermalization processes.

This inherent response comes from the fact that most of the photothermal detection methods are using a matrix density change by the temperature increase as the source of the signal. In an effort to understand the thermalization from a point of view of the translational energy of the solvents, we recently developed four new methods: temperature lens,[26–28] temperature grating,[26,29,30] an acoustic peak shift method[32–33] and molecular heater-molecular thermometer system.[34,35] In this Account, I will review the principles of these measurements and present some typical results. The results showed that the temperature rise after the decay of the electronic state is quite fast in water. When the solvent motions are coupled strongly with the large energy fluctuation, that fluctuation may efficiently transfer the internal energy to the kinetic energy. Hence it is expected that the energy transfer depends on the nature of the solute–solvent interaction as well as that of the solvent–solvent interaction. The mechanism and the rate of the temperature rise were further explored in various systems by changing the matrices using the acoustic peak shift method. Finally, a new molecular integrated system: molecular heater-molecular thermometer, is described as a new trial for the study of the temporal and spatial propagation of the thermal energy from the "hot" molecules.

Principle

1. Temperature Lens (Temp. L). When molecules in solution are excited by a beam that has a Gaussian spatial form, the Gaussian temperature distribution can be created in solution through the photothermal effect. The temperature change induces a change of the refractive index, and the created Gaussian-type distribution of the refractive index acts as a "lens", which focuses or defocuses another probe beam (Fig.1a). The focus or defocus effect can be detected by monitoring the probe light intensity through a pinhole at a far field from the sample. Traditionally this type of experiment for detection of heat is called the thermal lens method.[18–21,36] One has not expected to observe this thermal lens signal in a fast time scale, because acoustic propagation of the illuminated region is required to create the density change, which is the dominant origin of the refractive index change by the heating. However, recently we have clearly shown that this method could detect the thermalization process in a very fast time scale. Not only that, we noticed that there are various origins for the refractive index change after photoexcitation, such as the thermal effect caused by the nonradiative transition,[18–21,26–28] creation of excited states or reaction products (population lens (PL)),[37–38] volume change of the molecules (volume lens),[39–40] solvent reorganization,[41] and the optical Kerr effect (optical Kerr lens (OKL)).[42] The created Gaussian type distribution of the refractive index caused by these various origins acts as a "lens". We called these lens signals "transient lens (TrL)" signal.[28,43] This TrL method provides a sensitive and quantitative measurement of heat with a rather simple setup.

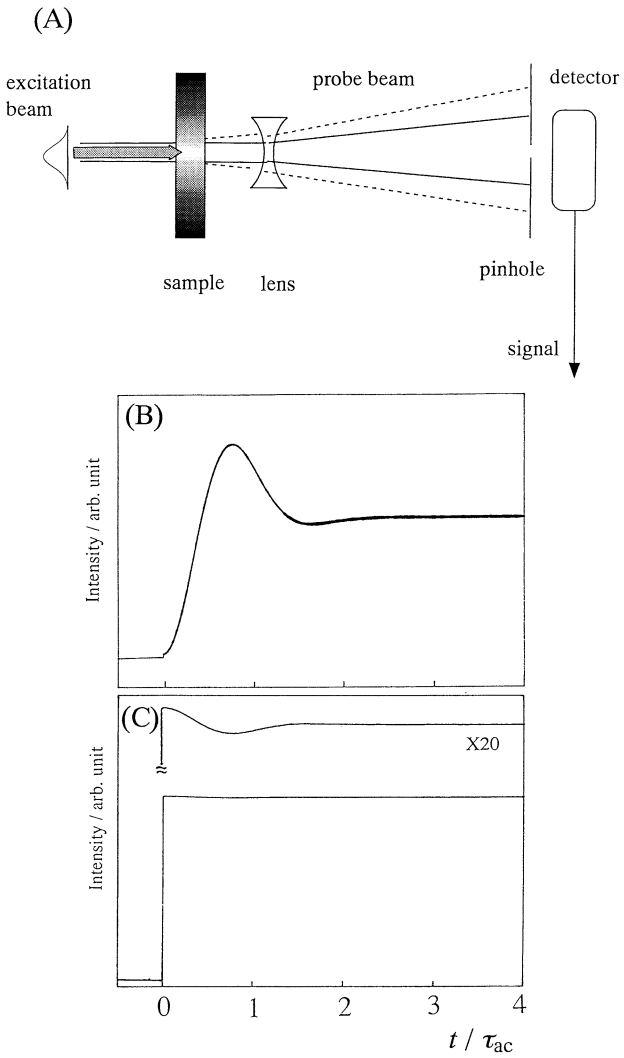

Fig. 1. (A) Principle and experimental setup of the transient lens method. The excitation beam creates "the transient lens (TrL)" inside the sample. The probe beam through the sample is expanded by an external lens (The path of the unperturbed probe beam is shown by the solid line). When a concave TrL is created in the sample, the probe beam is further expanded by this TrL (dotted line). The light intensity through a pinhole at a far field is detected. Calculated temporal profiles of the (B) density lens and (C) temperature lens signals.

For an intuitive understanding of the ultrafast heat detection, if one chooses the density ρ and temperature T as the variables, the variation of the refractive index (δn) can be expressed by

$$\delta n = \{(\partial n/\partial \rho)_T (\partial \rho/\partial T) + (\partial n/\partial T)_\rho\} \delta T. \quad (1)$$

The first term is the refractive index change accompanying the density change by the thermal expansion of the medium (we called it density lens (Dens.L)) and the second term is that without the density change. It is the first term of Eq.1 that induces the 'thermal lens' signal in many reports.[18–21] The most notable difference between the first and the second terms is the response time of the signal. The Dens. L signal rises with a

100 ns time scale because of the acoustic transit time of the photoilluminated region (Fig.1b), while the temperature contribution rises as fast as the temperature rises (Fig.1c). Hence, the lens signal observed in ps range should come from the second term and the rise part of the signal should represent the temperature increase. Although the magnitude of the second term compared with the contribution from the first term was questioned sometimes, we have obtained clear evidence for the detectable contribution of this term in water,[26,29,30] and, in many organic solvents as well.[44] This component is called the temperature lens (Temp. L) signal for the TrL experiment. (The molecular origin of this $(\partial n/\partial T)_\rho$ term was investigated using the transient grating technique.[29] From the solvent dependence of its magnitude, we concluded that the origin of $(\partial n/\partial T)_\rho$ is the interaction induced polarizability change of the solvent. Based on this model, the ultimate temporal response of the Temp. L signal is expected to be an order of molecular collision ($\sim$100 fs).)

The TrL signal, $S(t)$, is defined by

$$S(t) = \{I(n(t)) - I(n(\infty))\}/I(n(\infty)) \quad (2)$$

where $I(n(t))$ and $I(n(\infty))$ are the intensities of the probe beam through the aperture at a given delay time, t, between the pump and probe pulses and at sufficiently long time after the excitation, respectively. Sometimes the absorptive component contributes to the observed lens signal. The absorptive contribution can be eliminated by a method reported before.[38]

2. Temperature Grating (Temp. G). The transient grating (TG) signal in this Account can be understood by an intuitive picture of "intensity grating". A sinusoidal modulation of the light intensity is produced by the interference of two light waves with a parallel polarization. The fringe spacing, Λ, (Fig.2a) is given by

$$\Lambda = \lambda_{ex}/2\sin\theta \quad (3)$$

where 2θ is the angle between the two excitation beams and λ_{ex} is the wavelength of the excitation. The light-matter interaction creates the sinusoidal modulation in the refractive index (n) and the absorbance (k) caused by various factors described in the previous section. The grating is monitored by the diffraction efficiency of another time-delayed laser pulse. For a thick grating, the probe is brought in at an appropriate angle to satisfy the phase matching condition (the Bragg condition). Under a weak diffraction condition, the diffraction efficiency is proportional to the square of the variations in the refractive index (Δn) and absorption (Δk).[22]

The refractive index change by the temperature rise is again expressed by Eq.1. In a short pulse excitation case, an acoustic signal dominates in the TG signal by the first term of Eq.1 (density grating (Dens. G)) and it disturbs any fast detection of the temperature rise (Fig.2b). However, when we can use the second term in Eq.1 (temperature grating (Temp. G)), the time resolution is no longer limited by the medium expansion time but only by the pulse width of the excitation light (Fig.2c). Therefore, the ultrafast detection of the translational temperature becomes possible. (Although a theoretical calculation showed that the Temp. G signal should have acoustic and diffusive parts as the Dens. G component, the acoustic part is very small.[26] Therefore the signal rise of the Temp. G does not depend on the thermal expansion time.)

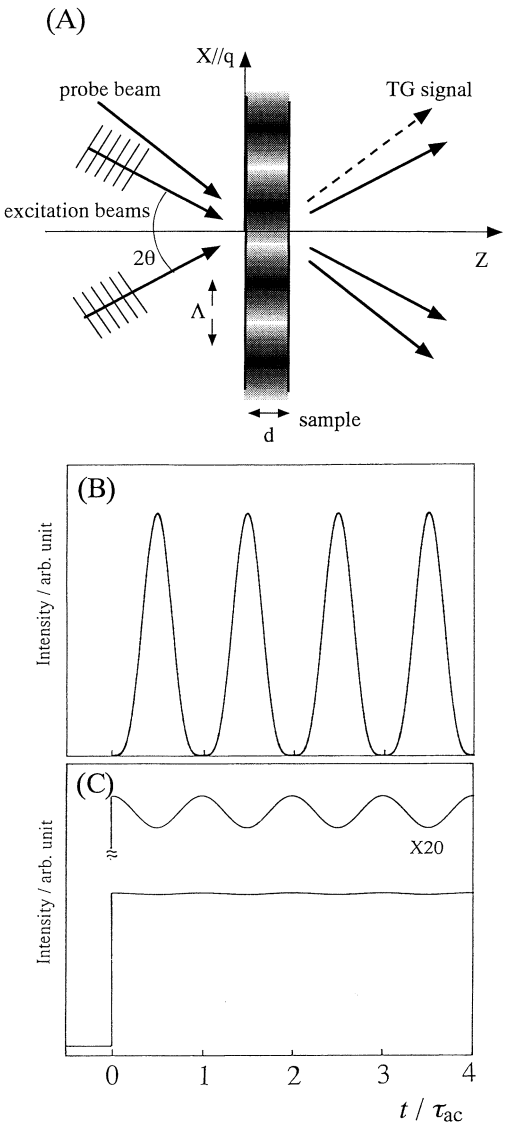

Fig. 2. (A) Principle of the transient grating method. Calculated temporal profiles of (B) the density grating and (C) temperature grating signals.

3. Acoustic Peak Delay Method. After the energy is deposited into the matrix under the grating illumination, the medium will expand periodically, which leads the sinusoidally modulated refractive index change (Dens. G) (Fig.2b). If the thermalization is slow, it will change the shape of the acoustic signal, which becomes apparent as a temporal delay of the signal. By a curve fitting of the acoustic signal, the rate of the temperature increase and the amount of the thermal energy may be extracted, as reported for a variety of systems.[22–25] However, if the rate is very fast, the difference in the acoustic temporal shapes for different rates is very subtle and it is almost impossible to determine the rate only from the temporal shape. A reasonable time resolution we may obtain by this curve fitting method could be one-tenth of the acoustic period

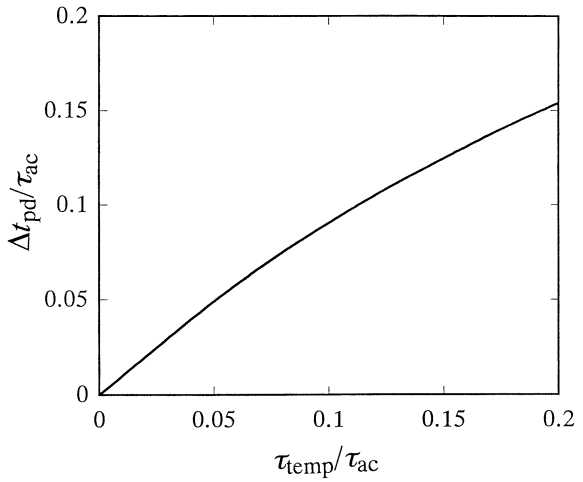

Fig. 3. Relation between the thermalization time (τ_{temp}/τ_{ac}) and the peak delay time ($\Delta t_{pd}/\tau_{ac}$) of the acoustic peak delay method.

τ_{ac} (= Λ/v (v: sound velocity)), τ_{ac} /10. For example, if the excitation beams at a wavelength of 320 nm is crossed at 30°, the acoustic period is around 600 ps and the time resolution could be ∼60 ps. This is not short enough for the study of the initial heating step. On the other hand, the acoustic oscillation shifts continuously with increasing the lifetime, and naturally the peak of the oscillation shifts with it. Experimentally, to determine the time at the peak position with a good accuracy is rather easy and it is expected that we can obtain the heating rate with a high time resolution (within a few ps accuracy) from the acoustic peak time. This is a principle of the acoustic delay method.

When the acoustic damping is neglected, the acoustic peak delay time (Δt_{pd}) is almost the same as the thermalization time (τ_{temp}) under a short τ_{temp} condition.[31] The calculated peak delays reduced by τ_{ac} at various τ_{temp}/τ_{ac} are plotted in Fig.3. The peak delay is almost linear up to the build-up time of $0.07\tau_{ac}$ (∼40 ps under our experimental conditions). The time delay also depends on the acoustic attenuation rate. If one increases the attenuation constant, the peak delay decreases. When there are two heat releasing processes with different lifetimes of τ_f and τ_s ($\tau_f < \tau_s$), the temporal profile of the acoustic signal should depend on these time constants as well as the releasing energy from these processes. Calculating the peak delay as a function of Q_s/Q_{tot} (Q_s; thermal energy from the slower process, Q_{tot} (= Q_s+Q_f); total thermal energy), we found that the acoustic peak shifts linearly with Q_s/Q_{tot} from Δt_{pd} for Q_{tot} = Q_f to Δt_{pd} for Q_{tot}= Q_s. If there are several thermalization processes, Δt_{pd} provides the energy weighted average thermalization time, τ_{temp}.[31] For example, if there are two thermalization processes with lifetimes of τ_f and τ_s, Δt_{pd} is given by

$$\Delta t_{pd} \approx (Q_f/(Q_f+Q_s))\ \tau_f + (Q_s/(Q_f+Q_s))\ \tau_s \qquad (4)$$

where Q_f and Q_s are thermal energies associated with the τ_f and τ_s processes, respectively. We measured the arrival times of the first (t_1) and the second (t_2) acoustic peaks. The temporal separation between the first and the second peaks ($\Delta t = t_2-t_1$) gives an acoustic frequency ω (= $2\pi/\Delta t$) in that solution as long as τ_i varies in a fast rate region. Next, Δt_{pd} was calculated by the relation of $\Delta t_{pd} = t_1-\Delta t/2$.

Experimental

The experimental details depended on the chemical systems we studied and also on the techniques we used. For the TG experiment, a short (picoseconds or subpicoseconds) pulse was split into three with two beam splitters. The frequency of the two beams was doubled and used as excitation beams. These beams were focused by lenses and crossed at about 30° inside the quartz sample cell in order to generate an optical interference pattern. The other pulse was used as a probe beam. The probe beam passed through an optical delay line was focused by a lens and brought into the sample cell by an angle that satisfied the Bragg condition. The diffracted TG signal was separated from other beams with a pin hole and a glass filter and detected by a photomultiplier. The detected TG signal was averaged with a boxcar-integrator and with a personal computer.

For the TrL experiment, a sample was irradiated by a focused pump beam. A collimated time-delayed probe pulse, which was generally nonresonant for any absorption band, passed through the irradiated region. The probe beam was expanded by another external lens (concave or convex lens) and the spatial deformation by the TrL effect was detected by a beam profiler or the light intensity change at the beam center (Fig.1a). The change of the light intensity (Eq.2) was plotted against the temporal delay between the pump and probe pulses.

Results and Discussion

1. Thermalization of Photoexcited Ni^{2+} in Water. First, the energy transfer rate from the electronically excited Ni^{2+} to the translational freedom of water molecules (solvent) is described. This ion was pumped by a ps-IR pulsed laser light and the thermalization time was measured by the Temp. L component in the TrL signal.[27] The lens signal appeared just after the photoexcitation within a few ps and decayed in the hundreds of milliseconds time scale. The observed lens signal in this wide time range ($10^{-12} \sim 10^{-1}$s) was completely analyzed. During 100 ns to 100 ms, the lens signal was dominated by the density lens component. The decay of the signal represents the thermal diffusion process from the photoilluminated region. An interesting feature was observed in a ps time range. A temporal profile of the TrL signal under the parallel polarization condition (E_{pump} // E_{probe}; $I_{//}$ signal) is shown in Fig.4a. Within the duration of the pump laser pulse, (which is shown in Fig.4c determined as explained below), the probe light was focused; that is, a convex lens was created in the solution. After the pump pulse left the sample, the probe light was defocused, which indicated the creation of a concave lens. A similar temporal profile was observed under the perpendicular condition ($E_{pump} \perp E_{probe}$; $I_{\perp}$ signal) (Fig.4b). In this case, the initial convex lens signal was weaker than that of the $I_{//}$ signal.

There are several physical processes which may give rise to the lens signal as noted in section 2.1. Among them, Dens. L, Temp. L, optical Kerr lens, population lens (PL) may be important under the present experimental conditions. We next consider these possibilities. First, the Dens. L signal should not contribute to the signal in this time scale because it should rise with a time constant of around 100 ns. This time response

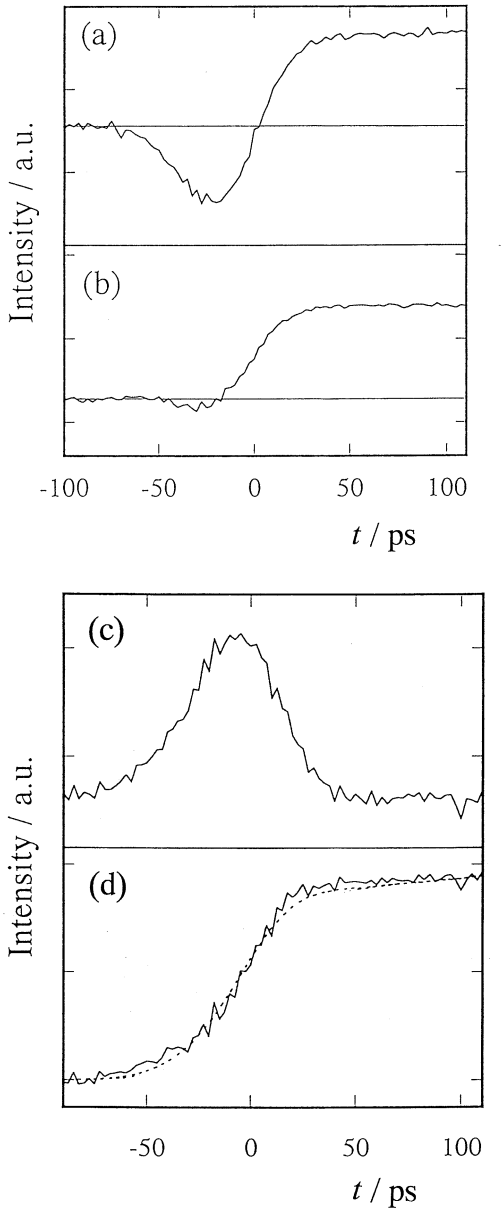

Fig. 4. TrL signals observed after the photoexcitation of Ni^{2+} in water under (a) the parallel polarization condition ($I_{//}$ signal) and (b) the perpendicular polarization condition ($I_{\perp}$ signal). (c) Optical Kerr lens signal and (d) Temp.L signal obtained from the $I_{//}$ and $I_{\perp}$ signals. The dotted line in (d) is a fitted line of the signal rise by a single exponential function with a lifetime of < 2 ps.

comes from the fact that the density cannot change instantaneously but it requires a passage time of the acoustic wave from the photoexcited region.[18,28] Second, the optically induced birefringence (optical Kerr effect) can create the transient lens signal in a fast time scale as shown before.[42] Based on the Born-Oppenheimer approximation, the magnitude of the nonlinear refractive index change due to the electronic response (δn_{ele}) with $I_{//}$ and $I_{\perp}$ is given by [45]

$$\delta n_{ele}\,(I_{//}) = 3\delta n_{ele}\,(I_{\perp}) \qquad (5)$$

and this relation has been indeed observed previously by the TrL method under the nonresonant pumping conditions.[42] The initial (spike-like) convex type lens signal observed during the pump pulse was attributed to the so-called optical Kerr lens signal induced by the electric field of the pump light.[42]

The intensity of the concave lens signal after the Kerr lens signal did not depend on the polarization condition. When the $I_{//}$ signal was subtracted from the $I_{\perp}$ signal, $I_{//}-I_{\perp}$, it gave the same profile as a response function of our system, which was determined by the pulse width of the laser (Fig.4c). This is consistent with the conclusion that the optical Kerr lens signal is due to the electronic response of water.

The electronic Kerr lens signal can be eliminated by taking the linear combination of $I_{//}-3\ I_{\perp}$. The residual signal is shown in Fig.4d. It rose within the pump pulse, gradually increased in a 500 ps time scale, and remained at almost a constant intensity up to 4 ns. The relatively slow rising (500 ps) was attributed to the relaxation from the metastable state of Ni^{2+}.[27]

It is rather difficult to completely exclude the possibility of the PL contribution in the observed signal. However, we could conclude that the contribution of PL should be minor compared with the Temp. L component as follows. Previously the ratio of $(\partial n/\partial T)_{\rho}$ to $(\partial n/\partial \rho)_T(\partial \rho/\partial_T)$ was measured for water.[29] If the PL contribution was significant in the signal, the signal intensity should be different from that expected from this ratio. On the contrary, we found that the ratio of the signal intensity in the fast time scale to that of the density lens signal agreed well with the reported one. Hence, the observed concave lens signal in the ps time scale was attributed to the Temp. L. signal. The very rapid rise of the Temp. L indicates that the temperature after the photoexcitation rises very fast. The instrumental response function (laser pulse) allowed us to estimate the rise time by the convolution method. The rapid increase of the signal during the pump pulse gave a longer limit of 3 ps for the energy transfer from Ni^{2+} to the solvents. This result showed two interesting points: the deactivation of the photoexcited Ni^{2+} in water should be very fast and the translational energy increases immediately after the deactivation of the electronically excited state.

The energy transport process may be described as follows. The ion and the surrounding water can be considered as a supramolecule. After the deactivation from the electronic state of Ni^{2+}, the energy will be transferred to the vibrational and translational energy of the water molecules in the first solvent shell, and these water molecules become 'hot' within a few ps after the deactivation. The energy of the hot spot is then transferred to the second shell of water and then to the third shell. Finally the temperature should be completely averaged in the photoirradiated region. Our result presented here indicates that the energy transfer process to the first shell of water completes within a few ps.

2. Thermalization of Proton Transfer Systems.

(a) Thermalization of HBP by Temp.G and Temp. L. If the relaxation rate of the photoexcited state is slow, this relaxation rate becomes the rate determining step of the thermalization. To investigate the intrinsic thermalization process, it is preferable to use a molecule of which the excited state lifetime

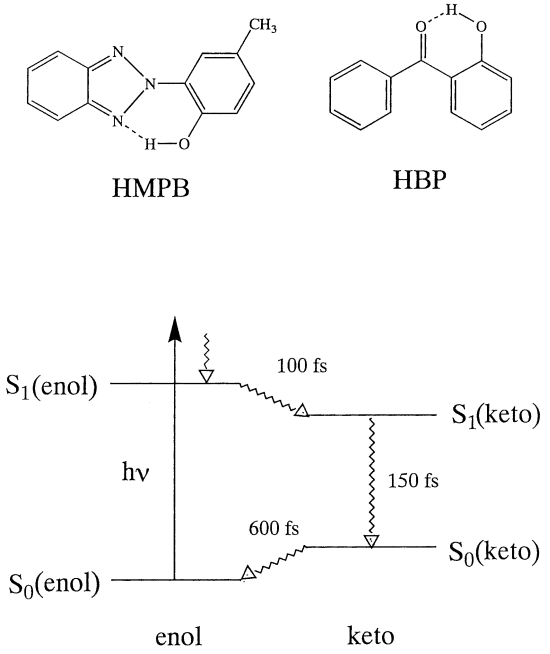

Fig. 5. Intramolecular proton transfer molecules we studied (upper) and the energy scheme of HMPB (lower).

is sufficiently short (less than a few ps). One of such molecules is an intramolecular proton transfer system (Fig. 5). For example, it is well known that the S_1 states of 2-(2-hydroxy-5-methylphenyl)-2*H*-benzotriazole (HMPB (commercial name: TIN)) and 2-hydroxyphenyl phenyl keteone (2-hydroxybenzophenone (HBP)) relax to the ground state very rapidly. After the photoexcitation of the enol form of HMPB, the excited state proton transfer occurs in a 100 fs time scale, followed by the radiationless deactivation of the keto-type S_1 (S_1(keto)) state with a time constant of 150 fs.[46,47] The keto-type ground (S_0(keto)) state molecule undergoes a proton back transfer to the enol geometry (S_0(enol)) with a time constant of 600 fs (Fig.5). HBP has been used as a calorimetric reference and a polymer photostabilizer, because of the rapid dissipation of the energy of the photoexcitaion.[17] The lifetime of the S_1 state of the intramolecularly hydrogen bonded species in dichloromethane was reported as < 10 ps by the transient absorption measurement.[48] The lifetimes of the S_1 state were reported to be 6 ps in hexane and 30 ps in ethanol with the two photon fluorescence excitation method,[49] and < 4 ps in hexane and 7 ps in ethanol with the fluorescence measurement.[50]

The photophysical dynamics of HBP in water was investigated by the Temp. G method with a picosecond pulsed laser (pulse width ∼30 ps).[30] The TG signal from HBP at room temperature consisted of mostly the Dens. G signal. Decreasing the temperature, the Dens. G intensity decreased because $\partial\rho/\partial T$ in Eq.1 decreases with the temperature. The TG signals at various temperatures were fitted by a superposition of the Dens. G and Temp. G signals. At 4 °, the signal consisted of the pure Temp. G component because $\partial\rho/\partial T$ vanishes at this temperature. The rise profile was fitted by a single exponential function with a 6 ps rise time. Since the rate of the temperature increase cannot be faster than the relaxation rate of the excited state ($S_1 \rightarrow S_0$ internal conversion) and the lifetime of the S_1 state was reported as 4–6 ps (*vide infra*), we concluded that the rate of the temperature increase was limited by the $S_1 \rightarrow S_0$ internal conversion process. Hence the energy conversion rate from the vibrational manifold of the ground state to the translational manifold should be very fast (< a few ps).

As shown above, we found a rapid thermalization from Ni^{2+} and HBP in aqueous solution. How about the rate in organic solvent? Since the intermolecular interaction between the solute and solvent should be different in water and in organic solvent, the solvent dependent experiment may provide us an important clue to understand the mechanism. However, the Temp.G method is hard to be applied to the organic solvent because the density component (Dens. G) dominates the signal at any temperature and it masks the Temp. G signal. The Temp. L, however, could be used because the rise of the Dens. L is slower (∼100 ns) and fast-rising Temp. L signal is not perturbed by the presence of the Dens. L signal.

In order to record the temperature increase in the time domain, we tried to detect the Temp. L signal in hexane.[44] Without the sample flow, the large Dens. L signal dominated and diffracted the probe light intensively. Hence we could not detect any time-dependent signal. However, by flowing the sample with an appropriate speed, the Dens. L could be effectively removed from the observation range and we could detect a fast response-transient lens signal in an organic solution. The lens signal intensity after the photoexcitation of HBP in hexane under the parallel polarization condition ($I_{//}$ signal) varied as a function of the delay time between the pump and probe pulses, similar to the TrL signal of Ni^{2+} in water. Within the duration of the pump laser pulse, the light intensity after the pinhole started to decrease, which indicated the creation of a concave lens. The signal intensity gradually increased within about 50 ps time scale, and remained almost a constant up to 4 ns. The temporal profile under the perpendicular condition ($I_{\perp}$ signal) was almost the same as the $I_{//}$ signal, this fact indicates that we can neglect the optical Kerr lens signal.

The lens signal at a longer time scale (after ∼40 ps) cannot be the PL signal, because the photoexcited states of HBP should be completely relaxed with a lifetime of ∼4 ps. The observed intensity ratio between the picosecond lens component and the Dens. L component agreed with the value determined previously.[29] Therefore, it is reasonable to assign the lens signal to the refractive index lens due to the second term of Eq.1 (Temp. L). Furthermore, this signal was observed only when HBP was contained in the sample: such a result indicates that the heat energy should come from the deactivation processes of the excited states of HBP.

Based on the above assignment, the lens signal should represent the heating process of the solution by the relaxation of the excited HBP. We fitted the rise part of the signal by a superposition of the PL and Temp.L components. We found that the signal rise can be reproduced well by a two-step thermalization kinetics with lifetimes of < 1 ps and 30 ps. This is consistent with the results obtained from the acoustic peak delay time measurement shown below.

(b) Acoustic Peak Shift of HMPB. The thermalization rates of HMPB and HBP molecules in various solvents were measured by the acoustic peak delay method of the TG signal.[33] First the excited state dynamics of HMPB was studied

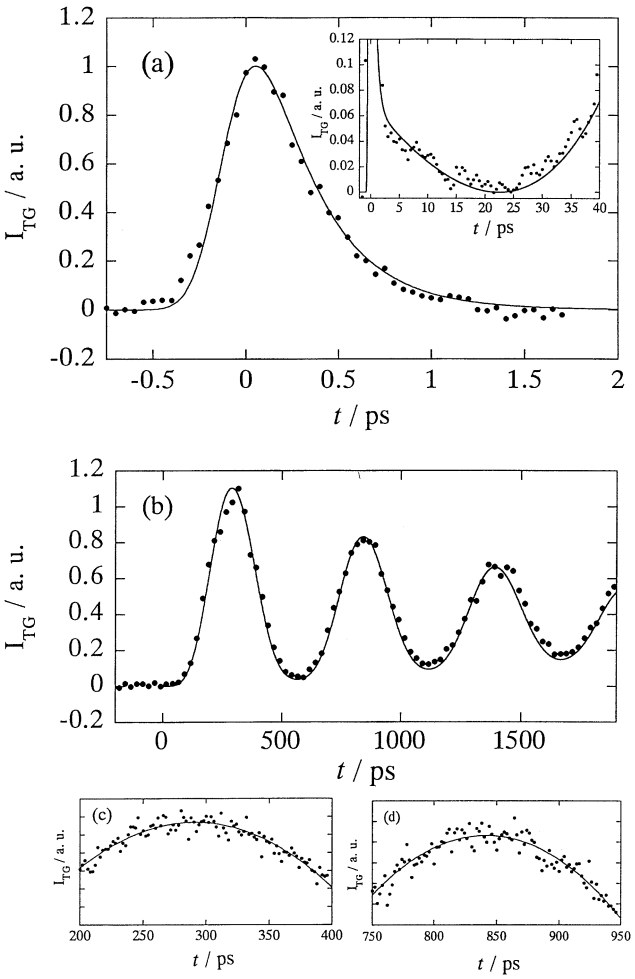

Fig. 6. (a) A typical PG signal and (b) an acoustic signal after the photoexcitation of HMPB (dotted line) and the best fitted calculated curves (solid line). (c) and (d) ; Profiles of the acoustic peaks (dotted lines) and the best fitted lines (solid lines).

by the population grating (PG) technique. After the photoexcitation of HMPB in cyclohexane a rather weak TG signal was observed in a picosecond time scale (Fig.6a). This signal should be assigned to the PG signal due the creation of the photoexcited states. This temporal profile was fitted well by a function of

$$I_{TG} = \alpha\{\delta n_f \exp(-t/\tau_f) + \delta n_s \exp(-t/\tau_s) + \Delta n_\rho\}^2 \quad (6)$$

where $\delta n_{f(s)}$, $\tau_{f(s)}$, and Δn_ρ are refractive index changes of the PG signal by the fast (slow) process, the lifetime of the fast (slow) process, and refractive index change by the density change (Dens. G), respectively. The lifetimes of the PG signal were determined to be $\tau_f = 600$ ($\pm$100) fs and $\tau_s \approx 30$ ps. The lifetime $\tau_f = 600$ fs agrees well with the lifetime of S_0(keto) of HMPB.[46] The very rapid rise of the PG signal was also consistent with the ultrafast creation of the S_0(keto) state with a lifetime of 150 fs (Fig.5).[46] Therefore we attributed the origin of the PG component to the S_0(keto) of HMPB. The 30 ps dynamics was attributed to the cooling process of HMPB (S_0(enol)) (decay of the hot band).

The acoustic TG signal of HMPB in cyclohexane is shown in Fig. 6b. The solid curve represents the calculated signal with $\omega = 1.14\times10^{10}$ s^{-1}. To find the acoustic peak times (t_1 and t_2), the signals around the first two peaks were recorded in detail (Fig. 6c, 6d). The time profiles around the peaks were fitted by the functions $A(t-t_i)^2+B$, where A and B are constants and $i = 1$ and 2 for the first and second peaks, respectively. The acoustic frequency (ω) and the peak delay (Δt_{pd}) were calculated from these t_1 and t_2 as described in section 2.3. After the correction for the acoustic attenuation rate, Δt_{pd} was found to be 20 ps.

After photoexcitation to the S_1(enol) state, HMPB shows a simple and fast photo cycle; HMPB returns to the ground state within 1 ps and the temperature of HMPB is elevated. [46,47] If all of the excess energy is dissipated to the solvents with one time constant, the thermalization time should be the same value as Δt_{pd}, which is 20 ps (Table 1). In this case, photoexcited HMPB should relax to the thermally equilibrium state with a lifetime of 20 ps. However, a 30 ps cooling dynamics of HMPB was clearly observed in the PG signals. Therefore it is unlikely that all of the excess energy is dissipated to the solvents with one time constant, that is, there are more than two thermalization kinetics. From this consideration, the vibrational cooling time observed in the PG signal (30 ps) should be one of the thermalization times. By assuming that the lifetime of the faster process (τ_f) is 1 ps (or it could be faster because the PG signal does not clearly show the dynamics after 1 ps), one can calculate the amount of the thermal energies associated with these two processes (Q_f and Q_s for $\tau_f = 1$ ps and $\tau_s = 30$ ps, respectively) from the observed Δt_{pd} (Eq.4). For example, in cyclohexane, an energy of about 10000 cm^{-1} is dissipated by the fast process and the remaining energy (21000 cm^{-1}) by the slower (30 ps) process.

(c) Acoustic Peak Shift of HBP. Similar PG and acoustic signals were observed for HBP in hexane. The lifetimes of faster and slower PG components were found to be $\tau_f = 400$ ($\pm$ 50) fs and $\tau_s = 30$ ($\pm$5) ps, respectively.[33] It was found that Δt_{pd} after correction for the acoustic attenuation rate was 10 ps using the same method as HMPB. The time profiles of the TG signals in acetonitrile, hexane and cyclohexane solutions were very similar to that in hexane. The obtained time constants are summarized in Table 1.

In hydroxylic solvents such as ethanol, a similar kinetics was observed. For example, the time profile of the PG signal could be reproduced with $\tau_f = 400$ ($\pm$100) fs and $\tau_s = 3$–50 ps. From the acoustic signal, we found that the heating effect due to the intersystem crossing from the S_1 state to the T_1 state could be neglected under our experimental condition and the dominant relaxation mechanism in ethanol should be similar to that in the non-hydrogen bonding solvents. The peak delay time was determined to be 7 ps.

The kinetics of HBP is controversial and less clear. Among the reported different lifetimes of the S_1 state, we believe that the lifetime measured by the fluorescence detection (< 4 ps in a non-hydrogen bonding solvent and 7 ps in ethanol) is the most reliable based on several grounds.[33] Hence, the photophysical process of HBP can be summarized as follows; the photoexcited S_1(enol) state relaxes to the S_1(keto) state with a lifetime of

Table 1. The Lifetimes (τ_f, τ_s) of the Population Grating Signals, the Peak Delay (Δt_{pd}) of the Acoustic TG Signals and the Calculated Thermal Energies (Q_f, Q_s) by Assuming that the Thermalization Process Takes Place with Lifetimes of 1 ps and 30 ps Respectively

	τ_f/fs	τ_s/ps	Δt_{pd}/ps[a)]	Q_f/cm^{-1} [b)]	Q_s/cm^{-1} [b)]
HMPB/cyclohexane	600±100	∼30	20	10000	21000
HBP/hexane	400±50	30±5	10	20000	12000
HBP/cyclohexane	400±100	30±5	13	17000	14000
HBP /acetonitrile	400±100	30±5	12	17000	14000
HBP / ethanol	400±100	∼30	7	24000	7200

a) The error of Δt_{pd} is ± 3 ps. b) The errors of the Q_f and Q_s are ± 2000 cm^{-1}.

400 fs. The S_1(keto) state decays to the S_0(keto) state with a lifetime of < 4 ps in non-hydrogen bonding solvents and 7 ps in ethanol. The vibrational cooling process in the S_0 manifold takes place with a lifetime of ∼30 ps. The thermalization process should reflect these excited state dynamics.

If the entire thermalization occurs with a lifetime of 30 ps, Δt_{pd} should be 30 ps, which is quite a bit longer than the observed values, 7–13 ps in Table1. Therefore, similar to the case of HMPB, we must think that there are more than two thermalization kinetics. If we assume that the thermalization process can be described by two (∼4 ps and 30 ps) thermalization kinetics, the relative thermal energy from the entire thermalization processes can be calculated from the observed Δt_{pd} as Q_f = 20000 cm^{-1} and Q_s = 12000 cm^{-1} in hexane (Fig.7).

A simple and intuitive idea why we saw the two phase kinetics is that they represent the transitions between different electronic states or geometrical transformations. However, from a theoretical MO calculation, we concluded that the two distinct kinetics were not caused by the relaxation processes in different electronic states.[33] The faster process includes the vibrational relaxation in the S_1 state as well as in the S_0 state. The two different kinetics will be discussed in the next section.

(d) A Thermalization Model. We observed two step thermalization processes for HBP and HMPB in many organic solvents. This observation could be interpreted by two ways. First, the dynamics may be determined by the character of the intramolecular vibrational modes; that is, it may be possible that there are roughly two classes of vibrational modes; very short-lived vibrational states and relatively long-lived states. The former one is responsible to the faster heating and the latter one for the slower heating.

Second, the two-step thermalization could be related with the energy flow mechanism from the solute to the solvents. One of plausible mechanisms can be described as follows (Fig.8). Just after the internal conversion process, only the excited solute molecule possesses the excess energy. The energy is first transferred to several solvent molecules that are effectively coupled to the solute (doorway molecules; here we name the directly energy-accepting (DEA) solvents). The rate is expected to be proportional to the strength of the intermolecular interaction and the temperature difference between the solute (T_{solute}) and the DEA solvent (T_{DEA}). The energy transfer from the solute to the DEA solvent molecules is initially very fast, because the temperature difference between T_{solute} and T_{DEA} is large, and the rate is determined by the solute-solvent interaction. Subsequently, the temperature of the solute decreases, and that of the solvent increases. As the temperature difference becomes smaller, the energy transfer becomes slower. Subsequent energy flow from the solute to the solvent is determined by the thermal diffusion process from the DEA to the outer solvents (slow process). (In this case, the slower lifetime (τ_s) should depend on the thermal diffusivity of the solvent. However, since the difference in the thermal diffusivity among the solvents we examined is not large compared with the experimental uncertainty of τ_s, we cannot find the solvent dependence.)

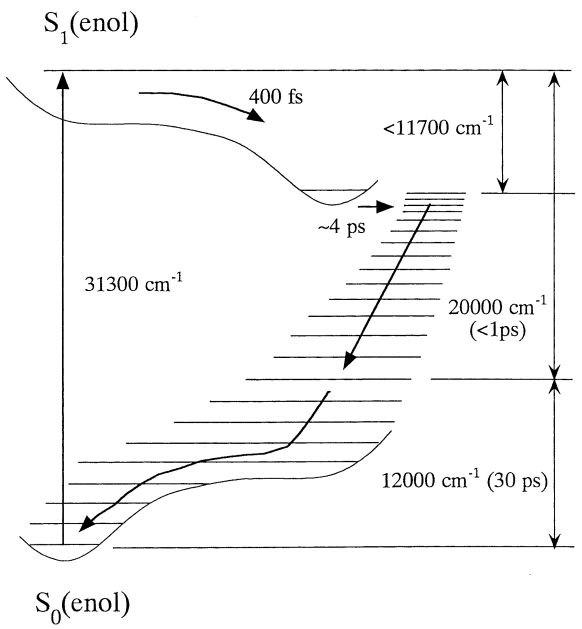

Fig. 7. Schematic illustration of the energy relaxation of HBP.

It may not be easy to distinguish these two possibilities experimentally. However, we think that the second explanation is more likely because of the following reasons. First, several different molecules are found to show the two-step thermalization processes, such as HBP, HMPB, stilbene,[6] porphyrins,[4] and 2,6-diphenyl-4-(2,4,6-triphenylpyridinio)phenoxide (betaine 30) (section 4.3). It is hard to imagine that all of these molecules accidentally have similar vibrational characters. Second, the thermalization scheme is sensitive to the solvent. Table 1 shows Q_f and Q_s of HBP in various solvents. Q_f was larger for alcoholic solvents. More clear correlation was observed for betaine 30 as described in the next section. It was found that the thermalization rate is enhanced by the hydrogen bonding. This solvent dependence may support the second

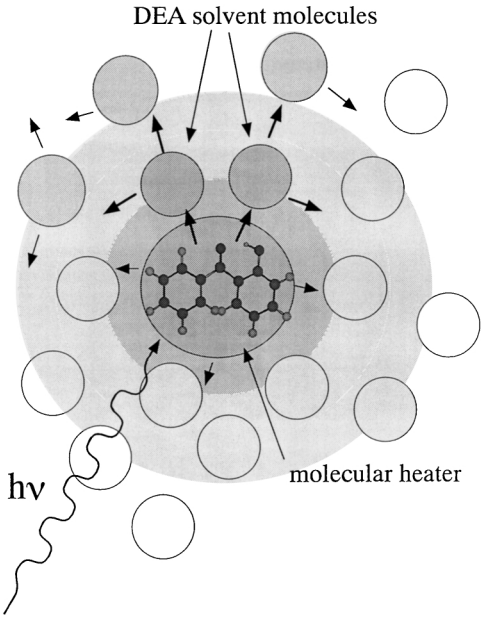

Fig. 8. Illustration of a thermalization model we used to explain the experimental observations. The energy of the photoexcited molecule is first transferred to doorway molecules (DEA solvent) and then diffused out to the bulk phase. The extent of shading represents the temperature.

mechanism because such a large solvent dependence may not be expected from the first mechanism. (The intermolecular interaction depends on the solute as well as the solvent. Hence, it should be noted that the rate of the faster process and the relative amplitude of the fast and slow heating processes should depend on the *solute* even if the second mechanism is dominant.)

The temporal profile of the heating process based on the later model can be calculated as follows. The energy of the solute is dissipated to the DEA solvents with two steps; $S_1^* \rightarrow S_1$ (S_1^*: the Frank–Condon state from the ground state) and $S_1 \rightarrow S_0$ energy relaxation (lifetime of τ_{S1}) processes. Since the $S_1^* \rightarrow S_1$ relaxation completes very quickly (less than 1 ps), the time evolution of this process can be neglected within our experimental time range and this process provides an initial temperature rise at $t = 0$. After that, the time evolution of the solute energy can be given by

$$C_{solute}\frac{dT_{solute}(t)}{dt} = C_{solute}\left\{-\frac{T_{\mathrm{solute}}(t) - T_{\mathrm{DEA}}(t)}{\tau}\right\} + \frac{Q_1}{\tau_{S_1}}\exp(-t/\tau_{S_1}) \quad (7)$$

where τ is the thermalization time, C_{solute} is heat capacity of the solute, Q_1 is the released energy by the internal conversion from the S_1 state. Here we assume that the thermal equilibrium among the translational mode is achieved very fast. The temperature change of the DEA solvent is given by

$$N_{DEA}\,C_{DEA}\frac{dT_{solute}(t)}{dt} = C_{solute}\left\{\frac{T_{\mathrm{solute}}(t) - T_{\mathrm{DEA}}(t)}{\tau}\right\} \quad (8)$$

where N_{DEA} is the number of the DEA solvent(s) and C_{DEA} is the heat capacity of the solvent. The energy flow process from the DEA solvent(s) to the bulk solvent is assumed to be described by the classical heat conduction. In these equations, τ and N_{DEA} are only unknown quantities to calculate the transient temperature.

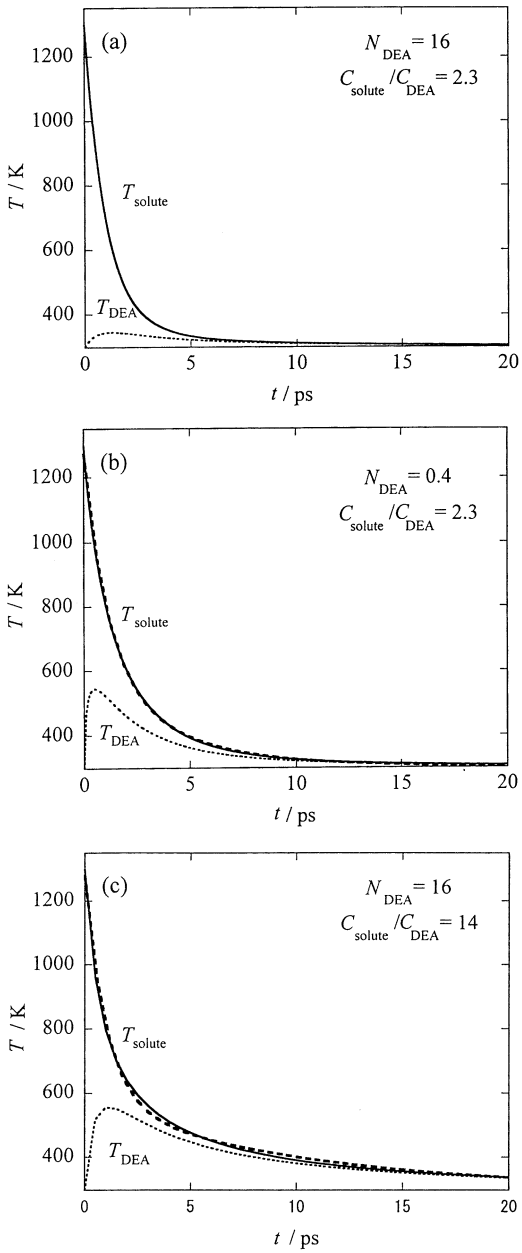

Fig. 9. A calculated transient temperatures of HMPB (T_{solute}: solid lines) and the DEA solvent (T_{DEA}: dotted lines) based on the thermalization model described in section 4.2. The parameters in the calculations are listed in the figures. The best fitted curve of T_{solute} by a bi-exponential function is represented by the broken line.

Since the lifetime of the S_1 state of HMPB is sufficiently short compared with the time resolution of the acoustic peak delay time, τ_{S1} was assumed to be 1 ps. In Fig.9a, the time evolutions of T_{solute} and T_{DEA} are shown for $\tau = 1$ ps and $N_{\mathrm{DEA}} = 16$, which is close to the number of the solvent molecules in the first solvent shell around the solute.[51] Here we used the

calculated C_{solute} and C_{DEA} at room temperature under the equilibrium condition. Interestingly, the time evolution of T_{solute} can be fitted very well by a biexponential function. The lifetimes of the faster (τ_f) and slower (τ_s) components are 1 ps and 15 ps respectively. As expected, the initial fast decrease of T_{solute} (Fig. 9a) is due to the heat releasing to the initially cold inner DEA solvent. T_{DEA} rises because of this energy transport and decays by the diffusion of heat to the outer sphere. However, quantitatively, using $N_{DEA} = 16$, the ratio of the amplitudes of these components (A_s/A_f) was too small to explain the observed Δt_{pd}. This ratio became closer to the experimental ratio ($Q_s/Q_f = 2$), when N_{DEA} was decreased. For example, the transient temperature can be fitted by a biexponential function with $\tau_f = 1$ ps, $\tau_s = 5$ ps, $A_s/A_f = 0.4$ for $N_{DEA} = 0.4$ (Fig.9b).

The ratio is also changed by changing C_{DEA}. In a fast time scale, all vibrational freedoms may not be equilibrated. In this case, the heat capacity should be smaller than that under the equilibrium. (If the energy of the all vibrational freedom is not equilibrated, the vibrational temperature may not be well defined. However, for the discussion here, only the fraction of the energy storage in the solvent molecule is essential.) For an extreme case, if all of the vibrational freedoms are completely neglected (i.e., only the translational and the rotational modes contribute to the heat capacity), the heat capacity of cyclohexane is 4 times smaller than the C_{DEA} we used. If one uses this value, the ratio became $A_s/A_f = 0.4$ with $\tau_f = 1$ ps, $\tau_s = 10$ ps (Fig.9c). All vibrational modes may not be neglected even for the transient temperature and N_{DEA} less than 1 is unrealistic. Therefore, the above two model calculations should be considered as extreme limits. Both calculated temperature changes gave still smaller A_s/A_f than the experimentally determined ratio ($Q_s/Q_f = 2$). In a real system, it may be possible that both effects, small N_{DEA} (< 16) and small C_{DEA}, could simultaneously contribute to increase the amount of the energy of the slow process.

The time profile of the heat releasing from HBP is more complex because the lifetime of the S_1 state cannot be neglected and the S_1 state acts as a time-delayed heat source. The time evolutions of T_{solute} and T_{DEA} are shown in Fig. 10a for $\tau = 1$ ps, $C_{solute}/C_{DEA} = 1.6$, and $N_{DEA} = 16$. The thermalization rate and the experimentally observed acoustic peak delay are related to the time dependence of the energy coming out from the solute, $Q(t)$, which is shown in Fig. 10b.[52] Again, the heating process was described roughly by two processes, faster one (4 ps) and slower one (18 ps). This feature qualitatively explains the observation, but, quantitatively the calculated contribution of the slower step is much smaller than the observed one. This ratio became much closer to the experimental value when we decreased N_{DEA} (Fig. 10c) or C_{DEA} (Fig. 10d).

In ethanol, the lifetime of the S_1 state is very similar to Δt_{pd} (= 7 ps), so that the observed Δt_{pd} can be reproduced with a large N_{DEA}. This result shows that the thermalization process should occur much more effectively in ethanol.

That N_{DEA} is smaller than the number of the solvent molecules in the first solvent shell ($\sim$16) is an interesting finding. Probably HMPB and HBP cannot interact strongly with all the solvent molecules that contact with the solute, but can be efficiently coupled to only limited members of the contacted solvents. Relating to this small N_{DEA}, an interesting energy re-

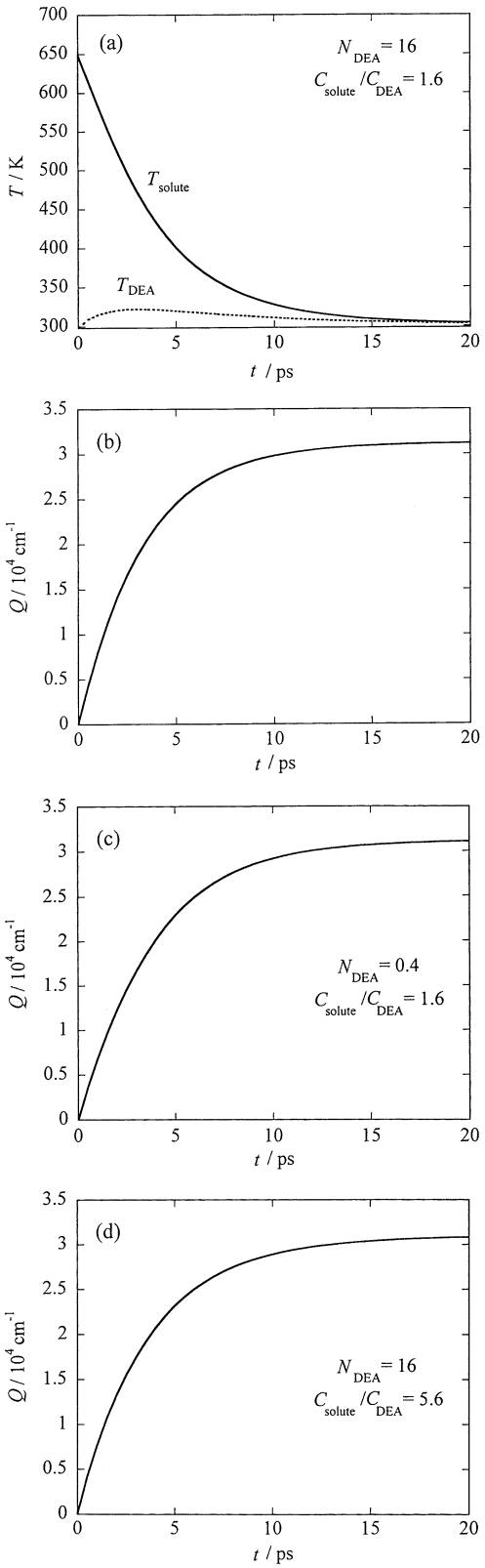

Fig. 10. (a) A calculated transient temperatures of HBP (T_{solute}) and the DEA solvent (T_{DEA}) based on the thermalization model described in section 4.2. Temporal profiles of the released thermal energy, Q, for (b) $N_{DEA} = 16$, and $C_{solute}/C_{DEA} = 1.6$, (c) N_{DEA}=0.4, and $C_{solute}/C_{DEA} = 1.6$, and (c) $N_{DEA} = 16$, and $C_{solute}/C_{DEA} = 5.6$.

leasing mechanism was proposed by Nagaoka et al. using the molecular dynamics calculation for a proton transfer reaction of formamidine in aqueous solution.[53] The reaction energy flows to or is donated from only a few water molecules, which are located in regions effectively coupled to the solute: a reaction site as well as a position where the water molecule can couple to the π electron of the solute. Experimentally, we found that the thermalization rate was enhanced by the hydrogen bonding between the solute and solvent, as described later (section 4.3). Since only a few solvent molecules can participate in the hydrogen bonding to the solute, this result may indicate that these few molecules receive the thermal energy through the hydrogen bonding interaction. It may be reasonable to speculate that the effectively coupled solvent molecules (the DEA solvent molecules) are located close to a functional group (e.g. carboxyl group). A theoretical study using such as the molecular dynamics is required to describe the thermalization process in further detail.

In summary of this section, the energy transfer from the solute to some solvent molecules is initially very fast, this is determined by the solute–solvent interaction. Gradually, the temperature difference becomes small, and the energy transfer becomes inefficient. Subsequent energy flow from the solute to the solvent is determined by the thermal diffusion process to the outer solvents. This process appears as the slower temperature increase. If the solute energy flows into all degrees of freedom (all vibrational, rotational, and translational modes) of all solvent molecules in the first solvation shell, the heat releasing completes very fast and the observed acoustic peak shift and Temp. L signal cannot be explained. Therefore, we think that the solute energy flows into not all of the solvent molecules in the first solvent shell, but only several molecules (doorway molecules or DEA solvent) are involved in the intermolecular energy transfer process. This efficiency and speed may be also related with the solvation structure as well as the intermolecular interaction.

3. Solvent Dependence of the Thermalization:Betaine 30. The rate of the thermalization and/or the number of the DEA solvents introduced in the previous section are considered to depend on the solute–solvent interaction. In order to examine the mechanism of the thermalization, we studied the solvent dependence of the thermalization rate using betaine 30 (B30) as a "molecular heater".[32] After the $S_0 \rightarrow S_3$ excitation, an extremely fast $S_3 \rightarrow S_1$ internal conversion was observed (< 200 fs) in all solvents we studied.[54,55] Subsequently the $S_1 \rightarrow S_0^*$ (S_0^*; isoenergetic (vibrationally excited) ground state) internal conversion takes place. The created S_0^* state vibrationally relaxes to the lowest levels, and this process deposits the thermal energy to the solvent modes. The $S_1 \rightarrow S_0$ internal conversion is slower, but fast enough so that the thermalization rate is not determined by the deactivation rate of the excited state. These photophysical properties make B30 suitable as the molecular heater to study the elementary step of the photothermal effect.

The S_3 state of B30 was photoexcited by a subpicosecond pulsed laser and the temporal development of the temperature increase was detected by the acoustic peak delay method. The acoustic signal rose gradually after the PG signal. The peak position was determined by the fitting of only the top of the oscillation and the acoustic frequency ω and the peak delay time τ_{pd} were determined. The peak delay Δt_{pd} was 8.4 $\pm$ 3 ps in methanol. In ethanol, the peak delay was slightly longer (10.3 $\pm$ 3 ps) than in methanol. When hexane was mixed into the methanol solution, Δt_{pd} became even longer. On the contrary, when water was mixed, Δt_{pd} became shorter.

Table 2. Peak Delay Time (Δt_{pd}/ps), Lifetime of the S_1 State (τ_S/ps), and the Thermalization Time (τ_{temp}/ps) of B30 in Various Solvents.

Solvent	Δt_{pd}/ps	τ_S/ps[a)]	τ_{temp}/ps
Methanol	8.4	4.7	6.1
Ethanol	10.3	6.1	7.4
2-Propanol	12.9	8.0	9.2
1-Hexanol	15.7	(15)[b)]	9.0
Methylpropanol	12.0	—	—
Acetonitrile	24	0.5	24
Acetone	21	0.7	21
Ethylene glycol	15	15	7.4
Ethanol:hexane (3:1)[d)]	12.5	(2.8)[c)]	9.7
Ethanol:hexane (1:3)[d)]	18	(2.8)[c)]	15.2
Ethanol:water (3:0.5)[d)]	10.7	(2.8)[c)]	7.9
Ethanol:water (3:1)[d)]	9.1	(2.8)[c)]	6.3
Ethanol:water (3:1.5)[d)]	7	(2.8)[c)]	5.2

a) Lifetimes from Ref. 54 and 55.
b) Averaged lifetime in pentanol and heptanol.
c) Assumed to be the same lifetime as that in ethanol.
d) Volume ratio of the solvents.

The observed Δt_{pd} should be interpreted by the energetic dynamics ($S_3 \rightarrow S_1$, $S_0^* \rightarrow S_0$) as well as the lifetime of the S_1 state (τ_S). In order to evaluate the thermalization time (τ_{temp}), the effect of the finite lifetime of the S_1 state should be corrected from Δt_{pd}. For this correction, the contribution of the S_1 lifetime was subtracted by using a relation of [32]

$$\tau_{temp} = \Delta t_{pd} - f_S \tau_S \quad (9)$$

where f_S is a fraction of the energy of the S_1 state ($E(S_1)$) in the total energy: $f_S = E(S_1)/h\nu$. The reported lifetimes of the S_1 state from the transient absorption were used for τ_S.[54,55] Thus calculated τ_{temp} values are listed in Table 2.

The two step thermalization process discussed in the previous section was also observed for B30. The PG signal as well as the transient absorption signals indicate the presence of the slower dynamics. For example, the PG signal in methanol showed 20 ps dynamics, which was assigned to the vibrational cooling process. If we assumed that the whole energy was transferred to solvent with 20 ps rate, the observed peak delay should be 20 ps, which is quite a bit longer than that observed(6.1 ps). Hence we concluded that a faster thermalization process should exist besides the 20 ps process. This two-step process may be explained by the thermalization model presented in section 4.2(d).

In order to reveal the mechanism of the thermalization, we looked for a correlation of τ_{temp} with a solvent property. When we plotted τ_{temp}^{-1} against N_{OH} (/10^{-2} mole number of OH group/cm^3), which is the number of hydroxy groups per unit volume (Fig. 11), the plot showed surprisingly good correlation. This fact may indicate that the hydrogen bonding be-

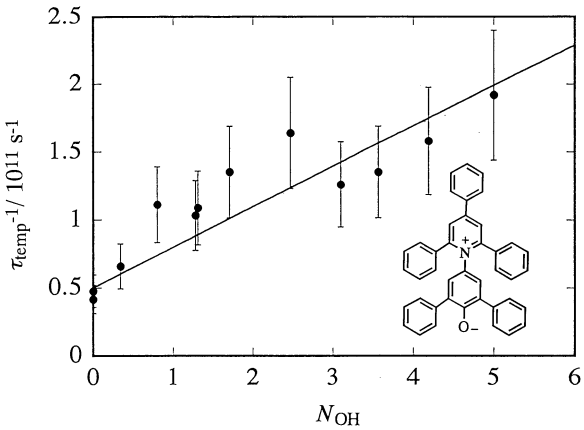

Fig. 11. A relation between τ_{temp}^{-1} of B30 and N_{OH} of the solvents.

tween the solvents and/or between solute-solvent enhances the rate of the temperature increase after the nonradiative transition. Indeed, the existence of the hydrogen bonding between B30 and alcohols was suggested[52] and it was found to play an important role in the solvation dynamics of B30 in protic solvents.

Why does the hydrogen bonding affect the thermalization process? We could consider two possibilities: increasing the intermolecular interaction between the solute and solvent and enhancing the density of low frequency modes. The strong intermolecular interaction could be an efficient pathway of the solute energy to the solvent. The low frequency modes will effectively couple with the translational mode of the solvent and the coupling will enhance the thermalization rate. The importance of the hydrogen bonding in relaxation phenomena has been suggested in several dynamics so far.[56-60] The vibrational lifetime of OH stretching mode was reported to be shortened by making the hydrogen bonding, which was explained by an effective relaxation channel of the bending vibration of the hydrogen bridge. An MD calculation showed that the energy dissipation in water is very fast.[60] The efficient intermolecular energy transfer results from the large energetic fluctuation of water which is coupled to the solute motion. From our studies, we concluded that the rate of the temperature rise: i.e., vibrational relaxation of many vibrational modes, is also enhanced by the hydrogen bonding.

In section 4.1, we found that the thermalization is very fast in water. It would be interesting to consider the solvent effect of water. If the plot of Fig. 11 is simply extrapolated to water ($N_{OH} = 11$), the thermalization rate is expected to be ~2.5 ps, which is the longest limit of the thermalization rate determined in water for Ni^{2+} (section 4.1). Therefore we think that one of the cause of the fast thermalization in water is the efficient hydrogen bonding capability of water. Recently, McDowell et al. measured the collisional vibrational relaxation of pyrazine in the gas phase and found that water is a very efficient relaxer of vibrationally excited pyrazine.[61] By a collision with water, about 3 times more vibrational energy was taken away compared with collision with CO_2. The effective energy relaxation by the collision of water agrees with our observation. Furthermore, I think that the high thermal diffusivity and a large heat capacity of water also play an important role of the efficient

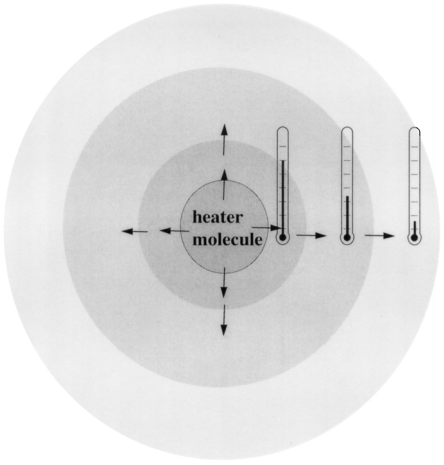

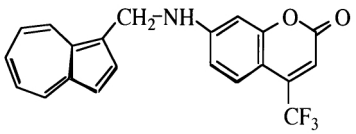

Fig. 12. Schematic showing how the transient temperature can be monitored with a high spatial resolution (upper) and the molecular integrated system we used (lower).

thermalization in water. The intermolecular hydrogen bonding between the solvent molecules may be the cause of the energy dissipation being efficient enough to take away the thermal energy from the solute.

4. Thermalization of Azulene. (a) Molecular Heater–Molecular Thermometer System. As discussed in the previous sections, the energy launched from the photoexcited solute initially heats up only several solvent molecules around the solute to make a local hot spot and this propagates in the matrix. After several 10–100 ps from the energy release, the energy propagation should be described by the macroscopic thermal diffusion equation. The temporal and spatial regions between just after the energy releasing from the excited molecule and the macroscopic heat transport regime are completely unexplored and will be a next interesting target in chemistry and physics of intermolecular energy transfer processes. We have constructed a new molecular heater-molecular thermometer integrated system for studying this process.[34,35] In this chemical system, a molecular heater that generates the thermal energy very fast was bound with a molecular thermometer, by which the transient temperature can be monitored. The heat flows at several distances from the solute can be monitored by changing the length of the bridge between molecular heater and thermometer (Fig. 12).

For a heater molecule, we chose azulene (Az) because the lifetime of the S_1 state is as short as 1 ps[62] and the vibrational relaxation in the ground state has been extensively studied already. [63-66] The thermalization process in the liquid phase was measured by monitoring the hot band of the $S_0 \rightarrow S_1$ absorption edge [65] and $S_0 \rightarrow S_3$ absorption edge.[66] For example, the vibrational cooling of azulene occurred with 11–13 ps in *n*-alkanes, 9 ps in ethanol, 3.3 ps in 3:1 mixture of water and meth-

anol, and 25.9 ps in $C_2Cl_3F_3$.[66] We can compare the temporal change of the solvent temperature with that of azulene itself.

Considering the spectroscopic characters, we chose 7-amino-4-(trifluoromethyl)coumarin (coumarin 151 (C151)) as a molecular thermometer because we could selectively photoexcite Az and the energy transfer from Az to C151 could be neglected. The center-to-center distance between azulene and the C151 moiety of this molecular integrated system (Az–CH_2–C151: Fig. 12) was estimated to be 0.65 nm from the optimized geometry calculated by a semi-empirical molecular orbital method. Hence the temperature of the thermometer should be elevated by the temperature of the solvent molecule in the first solvent shell, because the radius of azulene is 0.33 nm and the diameter of ethanol (one of solvents) is 0.43 nm. The 'temperature' of the thermometer was measured via change of the hot band absorption of C151.

The absorption spectrum of Az–CH_2–C151 was almost the same as the sum of the absorption spectra of azulene and of C151 except for slight red shifts ($\sim$10 nm). Hence, the intermolecular interaction between azulene and C151 in the ground state appears to be weak. We can photoexcite only azulene to the S_1 state using the laser light centered at 590 nm. The observed transient absorption spectrum of Az–CH_2–C151 in ethanol is shown in Fig. 13. The signal appeared just on the red edge side of the C151 absorption band. The time evolution of the transient absorption signal probed at 450 nm is shown in Fig. 13. The time profile of the transient absorption signal was almost identical at all the wavelengths in which the transient absorption signal appeared. The transient absorption spectra were also observed in acetone, 2-propanol and benzene. The spectra were very much similar.

This signal was attributed to the hot band of the C151 absorption based on several reasons.[34,35] A simple interpretation of the observed transient spectra is that the signal directly reflects the temperature rise of C151 due to the thermal energy dissipation from azulene. However, we must consider that the absorption coefficient (ε) is not generally proportional to the temperature. First, we examined the relationship between ε and T at the probe wavelength.

The hot band absorption appears due to the thermal excitation of higher vibrational levels in the ground state. The ratio of $\varepsilon(\nu,T)$ (ε at a wavenumber ν and at a temperature T) to that at room temperature (T_{rt} = 298 K) may be given by

$$\frac{\varepsilon(\nu,T)}{\varepsilon(\nu,T_{rt})} = \exp\{h(\nu-\nu_{00})(1/kT-1/kT_{rt})\} \qquad (10)$$

where ν_{00} is the wavenumber of the 0–0 transition and k is the Boltzmann constant. We fitted the data points in the red edge region by a linear function of ν with parameters of ν_{00} and T and determined $\Delta T = T-T_{rt} \approx 66 \pm 10$ K and $\nu_{00} \approx 22400$ cm^{-1}. The frequency of the 0–0 transition was reasonably close to that estimated from the absorption and the fluorescence spectra of Az–CH_2–C151 / ethanol (22500 cm^{-1}). This agreement supports the validity of this estimation and our interpretation that the induced absorption in this region comes from the thermal broadening of the 0–0 transition band of C151.

By using the determined ν_{00} (= 22400 cm^{-1}), we found that the temperature dependence of $\varepsilon(T)$ at the probe wavelength of 450 nm shows that ε is almost proportional to T in this temperature range. Therefore we concluded that the observed transient absorption signal intensity at 450 nm is directly proportional to the temperature change of the molecular thermometer.

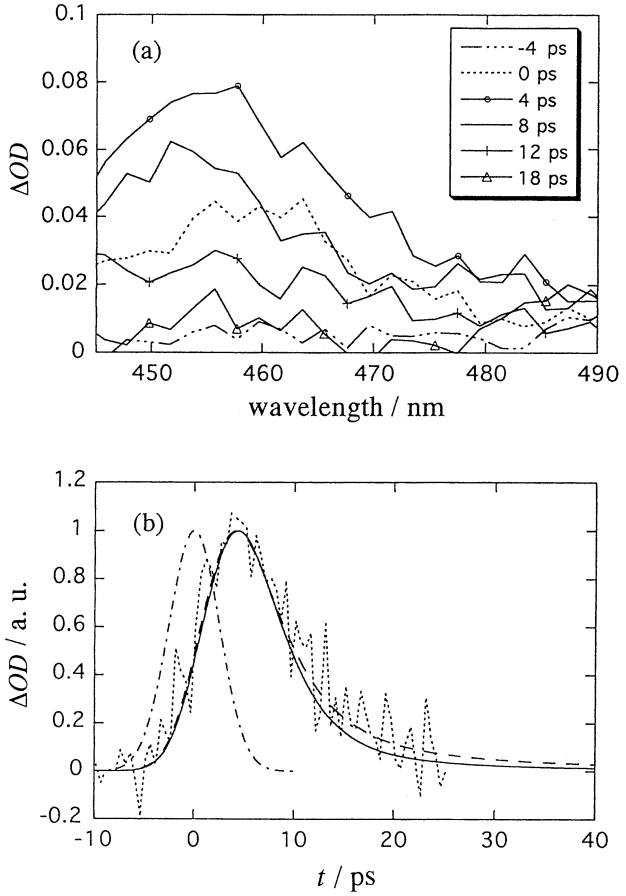

Fig. 13. (a) The transient absorption spectrum of Az–CH_2–C151 in ethanol. (b) The time profile of the transient absorption signal probed at 450 nm (dotted line). The solid line represents the calculated signal based on the thermalization model with the IVR process (τ_{IVR} = 5 ps and τ = 3 ps). The system response curve is represented by the point-dashed line. The fitted curve with the second thermalization model (without the IVR process) is also shown by the broken line (τ_{sum} = 3 ps).

(b) Models of the Thermalization Process. The transient temperature detected by the thermometer was analyzed using a thermalization model. The molecular thermometer can be heated up by two possible energy transfer mechanisms: through-bond and through-solvent mechanisms. The former process can be regarded as an intramolecular vibrational redistribution (IVR) process of the Az–C151 integrated molecule.

First, we used a simple thermalization model, which includes the IVR process with a lifetime of τ_{IVR} and through-solvent energy transfer with a lifetime of τ (Fig.14). For the through-solvent route, we considered several effectively coupled solvent molecules (DEA solvent molecules) as we introduced before. The DEA solvents should locate in the first solvent shell of the azulene–coumarin integrated molecule.

The thermometer C151 receives the excess energy from

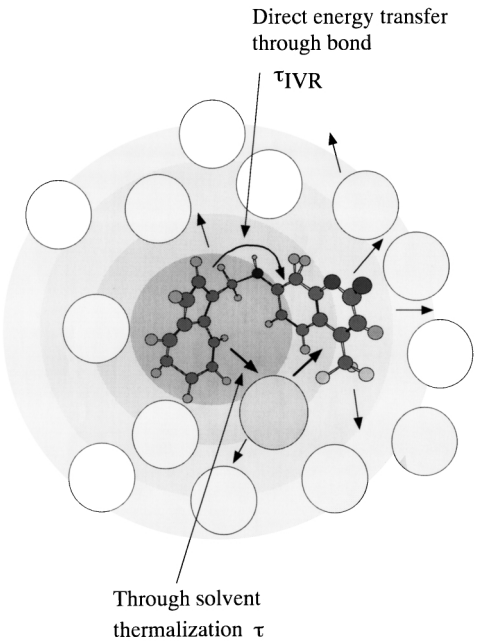

Fig. 14. A thermalization model including the through chemical bond and through solvent molecules. The extent of shading represents the temperature.

azulene directly and dissipates (or accepts) the energy to (or from) the DEA solvents. The thermalization model through the DEA solvent was the same as that explained before (section 4.2(d)). The energy is first transferred to the DEA solvent and, then the thermal energy of the DEA solvent diffuses to the outer solvents (which is assumed to be continuous) by the thermal diffusion. By adjusting τ_{IVR} and τ, we tried to reproduce the time profile of the signal and the temperature rise (ΔT). We found that the temporal profile can be reproduced well by several sets of these parameters. Considering the experimental value (66 K $\pm$ 10 K), we found that the signal was reproduced well with τ_{IVR} =5 $\pm$ 2 ps and τ = 3 $\pm$ 1 ps. The calculated signals are depicted in Fig.13b.

The obtained τ_{IVR} and τ indicate some characteristic features. First, although the IVR of large molecules in solution is believed to occur within a few ps, the observed τ_{IVR} were rather long: τ_{IVR} has to be longer than 3 ps in ethanol and 20 ps in acetone for explaining the temperature rise. Hence, the IVR process through the methylene bonds is not so fast as previously believed. Second, these τ_{IVR} strongly depended on the solvent. The thermalization occurred faster in the alcoholic solution. Third, the obtained τ was shorter than the previously reported vibrational cooling times of azulene. [63-66]

For a purpose of comparison, we constructed another thermalization model, in which the energy transfer through the σ-bond is neglected. In this model, the transient temperature at the thermometer molecule was calculated by the same model as section 4.2(d) and then convoluted with a response function of the thermometer. Here we used a single exponential function with a time constant of τ_{vib} as the response function. Using this model, it was found that the temporal profiles of the transient temperature of C151 calculated with the same τ_{sum} = τ+2.5 τ_{vib} gave very similar curves. Hence we can determine only τ_{sum} from the fitting of the observed profile. The best fit of the observed profile was obtained with τ_{sum} = 3 ps in ethanol (N_{DEA} = 16). However, the calculated temperature rise (∼10 K) was much lower than the observed rise (∼60 K). We may be able to improve the fitting by two ways. First, a slight contribution of the IVR process could increase the temperature. A model taking into account of the IVR process is the first model we presented above. Second, the higher temperature rise could be explained by a smaller N_{DEA}, as we used previously to explain the thermalization rate of HBP and HMPB. If we fitted the time profile with N_{DEA} = 2, ΔT was found to increase ∼30 K which was closer to the experimental value (66 $\pm$ 10 K). A possibility of the smaller N_{DEA} suggests that the energy transfer to the solvent is selective to a few DEA solvent molecules. A possibility of the small C_{DEA} for the transient temperature is also conceivable in this case.

From these two model calculations, we found that the observed transient temperature can be explained by the thermalization model with the IVR process or the model without IVR but with small N_{DEA} or small C_{DEA}. At present, we do not know which model is more appropriate for describing the thermalization of this system. However, in the first model, the solvent-dependent IVR process is hard to explain. Furthermore, if the IVR process through the σ-bond is important, the time profile of the transient temperature of the longer chain molecule, Az–$(CH_2)_3$–C151, is expected to be different from Az-CH2-C151, but this was not observed, as shown later. Here the thermalization model introduced in section 4.2(d) seems to be preferable.

It is important to stress that, by using either model, the thermalization process of Az–CH_2–C151 must be fast to explain the observations. The determined thermalization times (τ or τ_{sum}) are shorter than the vibrational relaxation time obtained by monitoring the vibrational temperature of azulene itself.[62] What could be the origin of the difference? One of the possibilities is that the coupling between the vibrational modes of azulene and the translational mode of the DEA solvents becomes strong due to the increase of the density of states around azulene by combining the methylene group and C151. The other possibility suggested is the participation of the non-uniform intramolecular vibrational relaxation. If the intramolecular vibrational redistribution is fast compared with the vibrational cooling process, the decrease of the solute temperature should be the same as the temperature increase monitored outside of the solute. However, if the intramolecular vibrational relaxation is not fast enough compared with the thermalization process, we should observe several kinetics in the thermalization process. For example, it could be possible that the hot band detection method in the previous studies monitored the populations of the vibrational levels with low vibrational quantum numbers, while the transient temperature detection in this study monitors overall energy transfer from azulene to the solvent. If most of the vibrational populations dissipate their excess energy to the solvents very quickly, the temperature of the solvent rises very fast and the minor part of the temperature rise could not be detected. On the other hand, the hot band detection of azulene is sensitive to the population dynamics of the vibrational levels with relatively large Franck–Condon factors to the S_1 state and the relaxation of these states could be

slow. To clarify the existence of the fast energy dissipation process, a photothermal spectroscopic study on the vibrational cooling of azulene is required.

What we did not expect was that the time profile of the transient absorption of Az–$(CH_2)_3$–C151 would be very similar to that of Az–CH_2–C151 except for the signal intensity. If the trimethylene chain is stretched out, the distance between azulene and C151 was estimated to be ∼11 Å from the semi-empirical molecular orbital calculation. In this case, the calculated time profile with the second thermalization model is clearly delayed and does not reproduce the observed signal. This result indicates that the C151 moiety should locate near the azulene moiety due to the flexibility of the trimethylene chain. One of notable differences was that the signal intensity of Az–$(CH_2)_3$–C151 is ∼3 times weaker than that of Az–CH_2–C151. The weaker intensity may come from two factors. First, the distances between azulene and C151 could be rather broadly distributed. From the signal intensity, we think that about ∼1/3 of C151 locates in the vicinity of azulene. Second, since the thermal energy is conducted in space, the temperature rise at a far distance from the molecular heater should be smaller than that at a closer distance. Hence, the compound that has a long distance between azulene and C151 cannot contribute to the transient temperature signal significantly. We think that these two factors make the time profile of the transient temperature of Az–$(CH_2)_3$–C151 similar to that of Az–CH_2–C151.

It may be interesting to study the transient temperature from compounds with a rigid spacer between the heater and the thermometer. Such molecular integrated systems will provide ideal systems for revealing the thermalization process with a high spatial resolution. A study along this line will be conducted in this group in future.

Summary

We studied the energy relaxation processes in solution after the deactivation of the electronic excited states. Using the time-resolved population grating, acoustic peak delay method and transient lens technique, we directly observe the time profile of the energy flow from the solute to solvent in ps time scale. The experimental setup of this Temp.L method is relatively simple and it will be used for tracing the time profile of the transient temperature for many other chemical systems. In aqueous solution, most of the thermalization completes within a few ps. In many organic solvents, the process proceeds roughly two phases: fast and slow. From a model calculation of the transient temperature, these two phase kinetics were explained as follows: the energy transfer to the first solvent shell molecules is the initial fast process and the thermal diffusion process from the hot solvent molecules to the bulk solvent molecules is the slower one. Based on a fact that the thermalization is enhanced by the hydrogen bonding, we think that the energy is transferred to solvent through a specific intermolecular interaction efficiently; that is, the intermolecular interaction increases the amount of energy of the faster process.

A part of this study was supported by the Grant-in-Aid (No.10440173) and the Grant-in-Aid on Priority Area of "Chemical Reaction Dynamics in Condensed Phase" (10206202) from the Ministry of Education, Science, Sports and Culture. The author is indebted to Prof. N. Hirota of Kyoto University and Dr. T. Okazaki of Nagoya University for the studies contained in this Account.

References

1 a) G. R. Fleming, "Chemical Applications of Ultrafast Spectroscopy," Oxford University Press, New York (1986). b) T. Elsaesser and W. Kaiser, *Annu. Rev. Phys. Chem.*, **42**, 83 (1991).

2 A. Seilmeier and W.Kaiser "Ultrafast Vibrational Energy Transfer in Liquids," in "Ultrashort laser pulses and applications," 2nd ed. by W. Kaiser, Springer-Verlag, New York (1993). Temperature lens and temperature grating in aqueous solution.

3 S. Sato and T. Kitagawa, *Appl. Phys. B,* **59**, 415 (1994).

4 Y. Mizutani and T. Kitagawa, *Science*, **278**, 443 (1997).

5 T. Nakabayashi, H. Okamoto, and M. Tasumi, *J. Phys. Chem. A,* **101**, 7189 (1997).

6 K. Iwata and H. Hamaguchi, *J. Phys. Chem. A*, **101**, 632 (1997).

7 S. L. Schultz, J. Qian and J. M. Jean, *J. Phys. Chem. A,* **101**, 1000 (1997).

8 P. Hamm, S. M. Ohline, and W. Zinth, *J. Chem. Phys.,* **106**, 519 (1997).

9 T. Lian, B. Locke, Y. Kholodenko, and R. M. Hochstrasser, *J. Phys. Chem.,* **98**, 11648 (1994).

10 a) F. Wondrazek, A. Seilmeier, and W. Kaiser, *Chem. Phys. Lett.,***104**,121 (1984). b) F. Laermer, T. Elsaesser, and W. Kaiser, *Chem. Phys. Lett.,* **156**, 381 (1989). c) A. Seilmeier, P. O. J. Scherer, and W. Kaiser, *Chem. Phys. Lett.,* **105**,140 (1984). d) A. Seilmeier, J. P. Maier, F. Wondrazek, and W. Kaiser, *J. Phys. Chem.,* **90**, 104 (1986).

11 T. Nägele, R. Hoche, W. Zinth, and J. Wachtveitl, *Chem. Phys. Lett.,* **272**, 489 (1997). U. Sukowski, A. Seilmeier, T. Elsaesser, and S. F. Fischer, *J. Chem. Phys.,* **93**, 4094 (1990). T. Robl, and A. Seilmeier, *Chem. Phys. Lett.,* **147**, 544 (1988).

12 a) S. Chen, I.-Y. S. Lee, W. A. Tolbert, X. Wen, and D. D. Dlott, *J. Phys. Chem.,* **96**, 7178 (1992). b) X. Wen, W. A. Tolbert, and D. D. Dlott, *J. Chem. Phys.,* **99**, 4140 (1993).

13 a) Y. Jiang and G. J. Blanchard, *J. Phys. Chem.,* **98**, 9417 (1994). b) Y. Jiang and G. J. Blanchard, *J. Phys. Chem.,* **98**, 9411 (1994).

14 S. A. Hambir, Y. Jiang, and G. J. Blanchard, *J. Chem. Phys.,* **98**, 6075 (1993).

15 M. S. Herman, J. L. Goodman, *J. Am. Chem. Soc.,* **111**, 1849 (1989).

16 A. M. Helms and R. C. Coldwell, *J. Am. Chem. Soc.,* **117**, 358 (1995); M. S. Churio, K. P. Angermund, and S. E. Blaslavsky, *J. Phys. Chem.,* **98**, 1776 (1994).

17 S. E. Braslavsky and G. E. Heibel, *Chem. Rev.,* **92**, 1381 (1992); T. Autrey, N. S. Foster, K. Klepzig, J. E. Amonette, and J. L. Daschbach, *Rev. Sci. Instrum.,* **69**, 2246 (1998); R. Schmidt, M. Schütz, *J. Photochem. Photobio. A*, **103**, 39 (1997); M. S. Herman and J. L. Goodman, *J. Am. Chem. Soc.,* **111**, 1849 (1989).

18 S. E. Bialkowski, "Photothermal methods for chemical analysis," Wiley, New York (1996).

19 H. L. Fang and R. L. Swofford, in "Ultrasensitive Laser Spectroscopies," ed by D. S. Kliger, Academic Press, NewYork, (1983).

20 S. R. J. Brueck, H. Kildal, and L. J. Belanger, *Opt. Commun.,* **34**, 199 (1980).

21 J. M. Heritier, *Opt. Commun.,* **44**, 267 (1983).

22 M. J. Eichler, P. Günter, and D. W. Pohl, "Laser Induced Dynamic Gratings," Springer, NewYork, (1986).

23 M. Terazima, *Adv. Photochem.,* **24**, 255 (1998); M. Takezaki, N. Hirota, and M. Terazima, *J. Phys. Chem.,* **100**, 10015 (1996); M. Takezaki, N. Hirota, and M. Terazima, *J. Phys. Chem. A,* **101**, 3443 (1997).

24 a) L. Richard, L. Genberg, J. Deak, H.-L. Chiu, and R. J. D. Miller, *Biochem*., **31**, 10703 (1992). b) L. Genberg, Q. Bao, S. Gracewski, and R. J. D. Miller, *Chem. Phys.,* **131**, 81 (1989).

25 K. A. Nelson, D. R. Lutz, and M. D. Fayer, *Phys. Rev. B,* **24**, 3261 (1981); E. Vauthey and A. Henseler, *J. Phys. Chem.,* **100**, 170 (1996).

26 M. Terazima, *Chem. Phys.,* **189**, 793 (1994).

27 M. Terazima, *J. Chem. Phys.,* **105**, 6587 (1996).

28 M. Terazima, *Israel J. Chem.,* **38**, 143 (1998).

29 M. Terazima, *J. Chem. Phys.,* **104**, 4988 (1996).

30 T. Okazaki, N. Hirota, and M. Terazima, *J. Phys. Chem. A*, **101**,650 (1997).

31 M. Terazima, M. Takezaki, S. Yamaguchi, and N. Hirota, *J. Chem. Phys.,* **109**, 603 (1998).

32 M. Terazima, *Chem. Phys. Lett.,* **305**, 189 (1999).

33 T. Okazaki, N. Hirota, and M. Terazima, *J. Chem. Phys.,* **110**,11399 (1999).

34 T. Okazaki, N. Hirota, T. Nagata, A. Osuka, and M. Terazima, *J. Am. Chem. Soc.,* **121**,5079 (1999).

35 T. Okazaki, N. Hirota, T. Nagata, A. Osuka, and M. Terazima, *J. Phys. Chem. A,* **103**,9591 (1999).

36 a) D. R. Siebert, F. R. Grabiner, and G. W. Flynn, *J. Chem. Phys.,* **60**, 1564 (1974). b) J. R. Barker and T. Rothem, *Chem. Phys.,* **68**, 331 (1982). c) M. Scotoni, M. Zen, D. Bassi, A. Boschetti, and M. Ebben, *Chem. Phys. Lett.,* **155**, 233 (1989). d) R. W. Redmond, K. Heihoff, S. E. Braslavsky, and T. George, *Photochem. Photobio.,* **45**, 209 (1987). e) F. R. Grabiner, D. R.Siebert, and G. W. Flynn,*Chem. Phys. Lett.,* **17**, 189 (1972). f) K. Fuke, M. Ueda, and M. Itoh, *J. Am. Chem. Soc.,* **105**, 1091 (1983). g) X. Song and J. F. Endicott, *Chem. Phys. Lett.,* **204**, 400 (1993). h) M. Terazima, T. Azumi, *Chem. Phys. Lett.,* **141**, 237 (1987); *Chem. Phys. Lett.,***153**,27 (1988). *J. Am. Chem. Soc.,* **111**, 3824 (1988); *J. Phys. Chem.,* **94**, 4775 (1990); *Appl. Phys. Lett.,* **57**, 1485 (1990). i) M. Terazima, H. Kanno, and T. Azumi, *Chem. Phys. Lett.,* **173**, 327 (1990).

37 M. Terazima and N. Hirota, *J. Phys. Chem.,* **96**, 7147 (1992); M. Terazima, *Chem. Phys. Lett.,* **230**, 87 (1994); M. Terazima, N. Hirota, H. Shinohara, and Y.Saito, *J. Phys. Chem.,* **95**, 9080 (1991).

38 M. Terazima, T. Hara, and N. Hirota, *J. Phys. Chem.,* **97**, 10554 (1993); M. Terazima, T. Hara, and N. Hirota, *J. Phys. Chem.,* **97**, 13668 (1993).

39 a) M. Terazima, T. Hara, and N. Hirota, *Chem. Phys. Lett.,* **246**, 577 (1995). b)T. Hara, N. Hirota, and M. Terazima, *J. Phys. Chem.,* **100**, 10194 (1996).

40 P. J. Schulenberg, W. Gärter, and S. E. Braslavsky, *J. Phys. Chem.,***99**,9617 (1995); M. Terazima, *J. Phys. Chem. A,* **102**, 545 (1998); S. Yamaguchi, N. Hirota, and M. Terazima, *Chem. Phys. Lett.,* **286**,284 (1998).

41 M. S. Churio, K. P. Angermund, and S. E. Braslavsky, *J. Phys. Chem.,* **98**, 1776 (1994).

42 M. Terazima, *Opt. Lett.,* **20**, 25 (1995).

43 M. Terazima, "Advances in multiphoton processes and spectroscopy," ed by S. H. Lin, A. A. Villaeys and Y. Fujimura, World Scientific, Singapore (1996), Vol.10, 1–96.

44 T. Okazaki, N. Hirota, and M. Terazima, *J. Mol. Liq.,* in press.

45 Y. R. Shen, "The principle of nonlinear optics," Wiley, NewYork, (1984); R. W. Hellwarth, Prog. *Quantum Electron.,* **5**, 1 (1977).

46 W. Frey and T. Elsaesser, *Chem. Phys. Lett.,* **189**, 565 (1992).

47 K. Lenz, M. Pfeiffer, A. Lau, and T. Elsaesser, *Chem. Phys. Lett.* **229**, 340 (1994); C. Chudoba, S. Lutgen, T. Jentzsch, E. Riedle, M. Woerner, and T. Elsaesser, *Chem. Phys. Lett.,* **240**, 35 (1995).

48 C. Merritt, G. W. Scott, A. Gupta, and A. Yavrouian, *Chem. Phys. Lett.,* **69**, 169 (1980).

49 K. J. Choi, L. A. Hallidy, and M. R. Topp, in "Picosecond Phenomena II," ed by R. Hochstrasser, W. Kaiser, and C. V. Shank, Springer-Verlag, Berlin (1980).

50 K. B. Eisenthal, "Ultrafast Chemical Reactions in the Liquid State," in "Ultrashort laser pulses and applications," 2nd ed., ed by W. Kaiser, Springer-Verlag, New York (1993).

51 The time profiles of the calculated transient temperatures in Fig.11 of Ref. 33 was not correct. Corrected figure is shown in Fig. 9.

52 The time profiles of the calculated transient temperatures in Fig. 12 of Ref. 33 was not correct. Corrected figure is shown in Fig.10.

53 M. Nagaoka, Y. Okuno, and T. Yamabe, *J. Phys. Chem.,* **98**, 12506 (1994).

54 N. E.Levinger, A. E. Johnson, G. C. Walker, and P. F. Barbara, *Chem. Phys. Lett.,* **196**, 159 (1991).

55 A. E. Johnson, N. E. Levinger, W. Jarzeba, R. E. Schlief, D. A. V. Kliner, and P. F. Barbara, *Chem. Phys.,* **176**, 555 (1993); R. J. Reid, S. Alex, W. Jarzeba, R. E. Schlief, A. E. Johnson, and P. F. Barbara, *Chem. Phys. Lett.,* **229**, 93 (1994).

56 R. J. Reid and P. F. Barbara, *J. Phys. Chem.,* **99**, 3554 (1995).

57 R. Inaba, H. Okamoto, K. Yoshihara, and M. Tasumi, *Chem. Phys. Lett.,***185**,56 (1991).

58 H. Okamoto, R. Inaba, M. Tasumi, and K. Yoshihara, *Chem. Phys. Lett.,* **206**, 388 (1993); J. Yu, M. Berg, *Chem. Phys. Lett.,* **208**, 315 (1993); R. Laenen and K. Simeonidis, *Chem. Phys. Lett.,* **292**, 631 (1998).

59 R. Laenen and K. Simeonidis, *J. Phys. Chem. A,* **102**, 7207 (1998); I. Benjamin and R. M. Whitnell, *Chem. Phys. Lett.,* **204**, 45 (1993); J. J. Shiang, H. Liu, and R. J. Sension, *J. Chem. Phys.,* **109** ,9494 (1998); D. Schwarzer, J. Troe, M. Votsmeier, and M. Zerezke, *J. Chem. Phys.,* **105**, 3121 (1996).

60 I. Ohmine, J. Chem. Phys., **85**, 3342(1986).

61 D. R. McDowell, F. Wu, and R. B. Weisman, *J. Chem. Phys.,* **108**, 9404 (1998).

62 D. Schwarzer, J. Troe, M. Votsmeier, and M. Zerezke, *J. Chem. Phys.,* **105**, 3121 (1996).

63 D. Schwarzer, J. Troe, M. Votsmeier, and M. Zerezke, *Ber. Bunsenges. Phys. Chem.,* **101**, 595 (1997).

64 D. Schwarzer, J. Troe, and M. Zerezke, *J. Chem. Phys.,* **107**, 8380 (1997); D. Schwarzer, J. Troe, and M. Zerezke, *J. Phys. Chem. A,* **102**, 4207 (1998); C. Hidelbach, I. I. Fedchenia, D. Schwarzer, and J. Schroeder, *J. Chem. Phys.,* **108**, 10152 (1998).

65 C. Hidelbach, J. Schroeder,D. Schwarzer, V. S. Vikhrenko, *Chem. Phys. Lett.,***291**, 333 (1998); D. Schwarzer, J. Troe, and J. Schroeder, *Ber. Bunsenges. Phys. Chem.,* **95**, 933 (1991).

66 B. D. Wagner, M. Szymanski, and R. P. Steer, *J. Chem. Phys.,* **98**, 301 (1993).

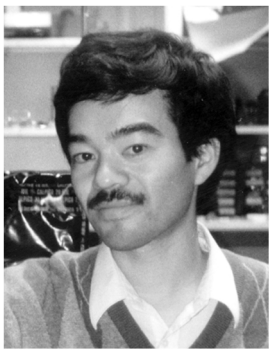

Masahide Terazima obtained his B.Sc.(1982), M.Sc.(1984), and Ph.D(1987) at Kyoto University. In 1986, he became a research associate in Tohoku University. In 1990, he moved to Department of Chemistry of Kyoto University as a lecturer and was promoted to an associate professor in 1993. His research interests include studies of energetics and molecular dynamics after photoexcitation of (relatively small) organic molecules as well as biological proteins in solution phase using several third order optical nonlinear spectroscopies.